Foam Front Displacement in Improved Oil Recovery in Systems with Anisotropic Permeability

P. Grassia

Department of Chemical and Process Engineering, University of Strathclyde, James Weir Building, 75 Montrose St, Glasgow G1 1XJ, UK

Abstract

A foam front propagating through an oil reservoir is considered in the context of foam improved oil recovery. Specifically the evolution of the shape of a foam front in a strongly anisotropic reservoir (vertical permeability much smaller than horizontal permeability) is determined via the pressure-driven growth model. The shape of the foam front is demonstrated to be extremely close to that predicted in the limiting case of a reservoir with no vertical permeability whatsoever, in particular any deviations from this shape are found to be second order in the ratio of vertical to horizontal permeabilities. Material points used to represent the foam front shape are shown to exhibit a uniform downward vertical motion, with a vertical velocity component which is proportional to the ratio of vertical to horizontal permeabilities. As the material points in question migrate downwards, they are replaced by new material points arriving from higher up, representing a long-time asymptotic solution for the front shape. This long-time asymptotic shape is sensitive to the ratio of vertical to horizontal permeabilities, with the foam front sweeping the reservoir less effectively as this ratio decreases.

Keywords:

Improved oil recovery; Pressure-driven growth; Foam in porous media; Permeability; Anisotropy; Mathematical modelling

Highlights

∗ Foam front propagation in an oil reservoir is considered via pressure-driven growth

∗ Strong anisotropy (vertical permeability much less than horizontal) is assumed

Email address: paul.grassia@strath.ac.uk (P. Grassia)

∗ Uniform vertical migration superposed upon primarily horizontal front motion

∗ Early-time front shape very insensitive to vertical to horizontal permeability ratio

∗ At long times front shape is quasisteady, and sensitive to permeability ratio

1. Introduction

During the oil and gas production process, oil and gas reservoirs gradually become depleted over time: as oil is extracted from the reservoir, the pressure inside the reservoir declines to the point at which it is no longer possible to extract any more oil under the reservoir's own internal pressure. Subsequently it is possible to inject fluids into the reservoir to raise the reservoir pressure again, and thereby enhance or improve production [1]. The injected fluid moves from an injection well to a production well, pushing along the reservoir's oil as it moves. One candidate fluid for injection is foam [2–4], which is believed to have a number of beneficial flow properties in the improved oil recovery context. One of these beneficial properties is [5] is the comparatively low mobility of foam, implying in turn a tendency to displace fairly uniformly through a porous medium (unlike more mobile injection fluids, such as e.g. water or air, that could be channelled along just a limited number of flow paths via fingering-type instabilities). Another beneficial property of foam [5] is trapping of foam films in pores that might have already been reached by preceding injection fluids (implying an ability to access parts of the reservoir which are not blocked by trapped films and which might not have been previously reached). For example, injection fluids such as water or air access large pores more readily than small ones. For injection utilising foam however, foam films might remain trapped in large pores but can collapse (and hence are not trapped) in smaller pores, since capillary pressure effects, causing the films to drain and collapse [5], are more significant in small pores.

In order to exploit foam injection operations more effectively, there has been considerable effort in the petroleum engineering community to simulate the foam improved oil recovery process using a number of rather sophisticated computer models [6–12]. An alternative approach introduced by Shan and Rossen [5], which has recently been dubbed pressure-driven growth [13], looks at a somewhat simpler phenomenological model.

As is more fully explained in [5, 13], the pressure-driven growth model attempts to repre-

sent the so called surfactant alternating gas process, which involves injecting first surfactant into the oil and gas reservoir followed by injecting gas (e.g. steam, carbon dioxide, nitrogen). A foam front is then formed in situ at the boundary between the surfactant and injected gas: see the sketch in Figure 1. The foam front displaces over time under the action of a net driving pressure: this is the difference between an injection pressure and a hydrostatic pressure.

The net driving pressure is balanced by dissipative forces, associated with moving the foam front through the reservoir. The dissipation tends to be localized in a wet foam zone where injected gas meets surfactant: the thickness of this zone might be as little as one percent of the distance over which the front itself has displaced [13]. As a first approximation then, the shape of the foam front (i.e. the shape of the wet foam zone) can be represented as a 1-D curve in a 2-D domain. The pressure-driven growth model specifically tracks the motion over time of material within this wet foam zone, with the shape of the foam front itself being reconstructed by tracking the motion of a multitude of material points covering the length of the front.

Some comments are pertinent. Since the hydrostatic pressure itself grows with depth, the net driving pressure diminishes with depth. This implies that points higher up on the foam front move further and faster than points lower down (see Figure 1). Moreover the implication is that there is a critical depth at which injection pressure and hydrostatic pressure come into balance: the foam front cannot advance beyond that depth.

Although the pressure-driven growth model was originally conceived to describe homogeneous and isotropic reservoirs [5], reservoirs are generally heterogeneous and anisotropic. The role of heterogeneity and anisotropy is unsurprising given that oil and gas bearing reservoirs are found within sedimentary rock formations, and such formations tend to be stratified into layers, the properties of each layer being sensitive to the conditions under which it was formed. During foam improved oil recovery, heterogeneity can affect the foam front shape by offsetting (or partly offsetting) the aforementioned tendency of points lower down on the front to move more slowly than those higher up. Anisotropy meanwhile causes points to move not normal to the foam front, but instead obliquely: see Figure 2. It soon became apparent [13] that the pressure-driven growth model could predict interesting behaviour in

the case of stratified reservoirs that were either heterogeneous [14] or anisotropic [15] or both. Specifically in the case of reservoir heterogeneity [14], solutions of the model can develop sharp concave corners (i.e. regions over which the orientation of the front changes quite suddenly over a comparatively small distance), and much of the challenge of obtaining solutions of the model numerically involves strategies for dealing with these concave corners. Particularly when heterogeneity is coupled to anisotropy, these sharp corners are found to move in very counter-intuitive ways [15].

The purpose of the present work is to consider anisotropy in the absence of heterogeneity, a situation which was first considered by de Velde Harsenhorst and co-workers [16, 17]. The key parameter governing anisotropy is the ratio between vertical and horizontal permeability of the reservoir. We denote this permeability ratio by the symbol κ_v and consider that its value can vary between zero and unity: e.g. [16] considered values of κ_v equal to 0, 0.01, 0.1 and 1. Specifically we set out in what follows to explain a curious result obtained by [16] when front shapes are computed numerically (details of the numerical technique and the results it produces are discussed in the cited reference). The finding (see the schematic sketch in Figure 3) was that the numerical data for $\kappa_v = 0.01$ and $\kappa_v = 0.1$ reported by [16] are very close to an analytical solution for the front shape applicable in the limit $\kappa_v = 0$. However numerical data for $\kappa_v = 1$ differed quite substantially from these other cases.

The rest of this work is laid out as follows. Section 2 describes the governing equations for pressure-driven growth in the presence of anisotropy. Then section 3 reviews a solution previously obtained in the literature [16, 17] in the case of extreme anisotropy $\kappa_v = 0$ (i.e. no vertical permeability whatsoever). After that the main novel results of the paper are presented, for the case of small but finite κ_v, both in terms of vertical motion (section 4) and in terms of a perturbed horizontal motion (section 5), demonstrating that the leading order perturbation vanishes. It is then shown (within section 6) how the solutions discussed back in sections 3–5 need to be replaced at long-times, and the behaviour of this long-time solution near the bottom of the front (section 7) and top of the front (section 8) is discussed. Finally section 9 offers conclusions.

2. Governing equations: Pressure-driven growth with anisotropy

The pressure-driven growth model [5, 13] as originally formulated for isotropic systems considers the motion within an oil and gas reservoir of a foam front formed at the boundary between injected liquid surfactant solution and injected gas. As is explained more fully in the appendix, the model is parameterised in terms of an operating parameter (the injection pressure P_{inj}), properties of the reservoir (porosity ϕ; permeability k) and also the properties of the foam itself (buoyancy $g\,\Delta\rho$ with g being acceleration due to gravity and $\Delta\rho$ being liquid-to-gas density difference; foam relative mobility λ_r, which is the reciprocal of an effective viscosity; residual water fraction in the foam S_w; and the ratio τ between the thickness of the foam front and the distance through which it has displaced).

As a recent extension of the work of Shan and Rossen [5], de Velde Harsenhorst and co-workers [16, 17] consider foam advance through a reservoir of anisotropic permeability: in this case, κ_v the ratio of vertical to horizontal permeability, becomes a relevant parameter, over and above the parameters mentioned previously. The governing equations are discussed in the appendix, where they are given in dimensional form. It is however convenient to make the equations dimensionless by scaling lengths by an amount $P_{\text{inj}}/(g\,\Delta\rho)$ (which represents the maximum depth d_{max} to which foam can penetrate) and times by an amount t_{scale} (which is defined in the appendix via equation (A.3), and which depends upon P_{inj}, ϕ, k, g, $\Delta\rho$, λ_r, S_w and τ). As is mentioned in the appendix, 'typical' values of d_{max} and t_{scale} could be respectively 265 m and 11 days, at least for the particular injection pressure 2.4×10^6 Pa mentioned in the appendix, although if the injection pressure is changed, both d_{max} and t_{scale} also change.

The governing equations (upon rescaling in dimensionless form with a subscript 'D' to denote dimensionless) become:

$$\frac{\mathrm{d}X_D}{\mathrm{d}t_D} = \frac{Y_D}{s_D \cos(\alpha - \beta)} \cos\alpha \tag{1}$$

$$\frac{\mathrm{d}Y_D}{\mathrm{d}t_D} = -\frac{Y_D}{s_D \cos(\alpha - \beta)} \sin\alpha\ \kappa_v \tag{2}$$

where $X_D \geq 0$ is the horizontal displacement of a front material point, $0 \leq Y_D \leq 1$ is the vertical coordinate of the material point (measured upwards from the bottom of the front), t_D is time, s_D is the path length travelled by the material point (with $\mathrm{d}s_D/\mathrm{d}t_D =$

$((\mathrm{d}X_D/\mathrm{d}t_D)^2 + (\mathrm{d}Y_D/\mathrm{d}t_D)^2)^{1/2})$, κ_v is the ratio of vertical to horizontal permeability, α is the angle that the normal to the front makes to the horizontal, and β is the angle that the instantaneous velocity vector of the front makes to the horizontal (see also Figure 2). By definition

$$\tan\beta = -\frac{\mathrm{d}Y_D/\mathrm{d}t_D}{\mathrm{d}X_D/\mathrm{d}t_D} \tag{3}$$

so that from equations (1)–(2)

$$\beta = \arctan\left(\kappa_v \, \tan\alpha\right). \tag{4}$$

Further explanation of equations (1)–(2) is given as follows. The term Y_D in the numerator on the right hand side of these equations reflects the fact that the net pressure driving the front along (i.e. injection pressure minus hydrostatic pressure) grows as one moves upwards, because the hydrostatic pressure falls. The term s_D in the denominator of equations (1)–(2) reflects the fact that a dissipative wet foam region at the foam front (across which pressure falls from injection pressure to hydrostatic) grows in extent as s_D grows, causing the front to slow down as it displaces further and further. Specifically the extent of this dissipative region measured along the direction of motion β is $\tau\, s_D$ where τ is a dimensionless parameter which is much smaller than unity, perhaps on the order of 0.01 [13], but with the exact value of τ being governed by foam collapse processes. The parameter τ is incorporated in the definition of dimensionless t_D causing τ to scale out of the governing dimensionless equations (although it appears in the dimensional equations given in the appendix). Note one curious feature of equations (1)–(2), namely the term $\cos(\alpha - \beta)$ in the denominator. This reflects the fact that the driving pressure gradient is driving pressure difference divided by front thickness, with the relevant thickness not being measured along the direction of motion β, but rather along the front normal direction α, and this latter thickness is smaller than $\tau\, s_D$ by a factor $\cos(\alpha - \beta)$ (see Figure 2). For a perfectly isotropic front, α and β of course coincide and $\cos(\alpha - \beta)$ is unity.

Equations (1)–(2) need to be solved with an initial condition. This is generally that $X_D = 0$ for all material points, regardless of the value of Y_D, and likewise $s_D = 0$ initially for all material points. Sometimes however (e.g. if one if trying to implement the equations numerically) it is simpler to set the initial s_D value to a small non-zero value [13, 18] (e.g. initial s_D equal to 0.01 or 0.001), as otherwise the predicted velocities diverge at initial time.

Introducing this small change to initial s_D has extremely little impact on the predicted front shape for subsequent times however (so we do not discuss it any further here). The governing equations are also generally solved with a boundary condition of horizontal motion of material points along the top boundary, i.e. $\beta = 0$ at the top boundary $Y_D = 1$. According to equation (4) for any non-zero value of κ_v at least, the condition $\beta = 0$ also implies $\alpha = 0$ at the top.

3. Analytic estimate of the front shape: zero vertical permeability

Special attention has been paid by [16] to the case of strong anisotropy where $\kappa_v \ll 1$: we shall focus upon that case also. An analytic formula for the front shape then becomes available and is reviewed here. As in [16], we make the following assumptions:

1. Materials points are instantaneously moving nearly in the horizontal, i.e. $\beta \ll 1$, which implies that $\cos(\alpha - \beta) \approx \cos\alpha$,
2. Material points have historically moved along paths nearly in the horizontal, so that $s_D \approx X_D$,
3. Material points have remained historically close to their current vertical location, so that Y_D is near constant.

Under these assumptions, it is possible to derive using equation (1)

$$\mathrm{d}X_D/\mathrm{d}t_D \approx Y_D/X_D \tag{5}$$

from which the formal $\kappa_v = 0$ solution of de Velde Harsenhorst and co-workers [16] (hereafter called the 'Velde solution') is derived

$$X_D \approx \sqrt{2Y_D t_D}. \tag{6}$$

This solution has a number of curious features.

First of all it exhibits 'poor reservoir sweep', i.e. points lower down on the front tend to be a long way behind the leading edge at the top $Y_D = 1$. A point at $Y_D = \frac{1}{4}$ for instance only has travelled half as far as the leading edge, and moreover the distance between this $Y_D = \frac{1}{4}$ point and the leading edge at the top grows unboundedly as time t_D grows.

Secondly the solution has the curious feature that $\alpha \neq 0$ at the top. Specifically according to the Velde solution

$$\tan\alpha \equiv \mathrm{d}X_D/\mathrm{d}Y_D \approx \sqrt{t_D/(2Y_D)}, \tag{7}$$

where the derivative $\mathrm{d}X_D/\mathrm{d}Y_D$ denotes a derivative along the foam front from material point to material point at a given time (as distinct from $\mathrm{d}X_D/\mathrm{d}t_D$ and $\mathrm{d}Y_D/\mathrm{d}t_D$ which are time derivatives following given material points). Clearly equation (7) predicts non-zero α for all Y_D including at the top ($Y_D = 1$).

Physically the top boundary condition we require is $\beta = 0$ (and the formal $\kappa_v = 0$ solution of course satisfies that because points only ever move horizontally when $\kappa_v = 0$). However for any non-zero κ_v, requiring $\beta = 0$ at the top, automatically imposes the condition $\alpha = 0$ also (see equation (4)). In the case of κ_v small but finite, there is presumably an adjustment region near the top across which the solution changes from a local $\alpha = 0$ solution, to a Velde-type solution (non-zero α) somewhere lower down: we will return to this point later.

Note that equation (7) is also problematic in the limit $Y_D \to 0$ since it predicts that the normal to the front becomes vertical there, which for any non-zero κ_v also implies material point velocities being vertical. This contradicts the assumption (used to obtain the Velde solution) that instantaneous front motion should be near horizontal. What is clear from equations (1)–(2) however is that in the limit as $Y_D \to 0$ there is very little motion of material points whatsoever regardless of direction, so this is not a limit that exhibits much in the way of interesting dynamics.

Returning to the case of a general Y_D, it is clear from equation (7) that if $t_D \gg 1$, then $\tan\alpha$ is much larger than unity, i.e. the front normal is now very far from horizontal, and the front itself is very far from its initial orientation which had $\alpha = 0$: this is again a manifestation of the poor reservoir sweep predicted by the Velde solution as time t_D increases.

This completes our review of the anisotropic permeability work of [16, 17]. In the sections to follow, we use this solution as the basis to derive a number of new results about pressure-driven growth systems with anisotropic permeability.

4. Vertical motion implied by the Velde solution

Although the Velde solution describes a primarily horizontal motion, we now proceed to demonstrate that, when one attempts to apply it to systems of very small but finite κ_v, it implies a weak superposed vertical motion as well. We can then use that weak vertical motion to investigate the validity of assumption 3 stated earlier.

We proceed as follows. If we substitute equations (6)–(7) into equation (2) using also assumptions 1 and 2, we obtain via the Velde solution

$$\frac{\mathrm{d}Y_D}{\mathrm{d}t_D} \approx -\frac{Y_D}{\sqrt{2Y_D t_D}}\sqrt{\frac{t_D}{2Y_D}}\kappa_v = -\frac{\kappa_v}{2}. \tag{8}$$

In other words the Velde solution predicts that all points regardless of their vertical height move downward at a rate $-\kappa_v/2$.

Equation (8) does break down at the bottom boundary of course, since no point can penetrate beyond $Y_D = 0$. Finding the exact trajectories that material points follow near $Y_D = 0$ is however of limited interest as there is little motion of any kind there.

Return therefore to consider equation (8) away from the bottom boundary. This equation actually provides a limitation on the time domain for the validity of the Velde solution: indeed we require time $t_D \ll O(\kappa_v^{-1})$ or else assumption 3 is violated (i.e. the value of Y_D sees large historical changes over times of order κ_v^{-1} or greater).

Consider now a time t_D much smaller than κ_v^{-1}, but still focussing on equation (8). Given that points initially on the front migrate downwards uniformly by an amount $\kappa_v t_D/2$ at time t_D, for times $t_D \ll O(\kappa_v^{-1})$ we could consider that most points on the front, i.e. those with $Y_D < 1 - \frac{1}{2}\kappa_v t_D$, have been on the front since the initial time (such as the Velde solution describes), whilst those with $1 - \frac{1}{2}\kappa_v t_D < Y_D < 1$ were introduced to the front more recently. Thus those points with $Y_D < 1 - \frac{1}{2}\kappa_v t_D$ might be considered to follow the Velde solution, whilst those points with $1 - \frac{1}{2}\kappa_v t_D < Y_D < 1$ constitute an adjustment region that deviates from the Velde solution, and somehow retains knowledge of conditions at the top boundary, and in particular the constraint that $\alpha = 0$ at $Y_D = 1$ for any finite κ_v: we shall return to consider a solution satisfying that constraint later.

5. Perturbation solution for horizontal motion

Now that we have first approximations to the horizontal and vertical motions of material points, it is possible to obtain an improved estimate of the horizontal motion of material points. The improved estimate is obtained via a technique similar to (albeit not identical to) a method already employed by [19]. The work of [19] applied to a system with isotropic permeability, but nevertheless managed to use the Velde solution as a starting point for a perturbation expansion of material point locations by considering sufficiently early times. Since by assumption the front itself is initially vertical along $X_D = 0$, the initial motion of material points is invariably horizontal (regardless of whether the system is isotropic or anisotropic). What is different in strongly anisotropic systems (with $\kappa_v \ll 1$) is that the approximation of near horizontal motion of material points remains applicable for considerably longer times than it does in isotropic ones.

The rationale for the procedure that we adopt is as follows. Recall that the horizontal motion of the front is strictly speaking described by equation (1), but we invoked a number of assumptions in section 3 to approximate this by equation (5). If we wish to obtain a more accurate representation of the horizontal motion, we need to improve upon the approximations that led to equation (5). The approach we take is a systematic extension to what has already been done in the foregoing sections: an initial assumption of no vertical motion whatsoever, led to a first approximation for the horizontal motion in section 3, which led in turn in section 4 to the conclusion that there was in fact a weak vertical motion, namely a downwards vertical drift with velocity component $\kappa_v/2$. Account must now be taken of this vertical drift, when attempting to improve the approximation for the horizontal motion. Observe that in an anisotropic system, as long as $t_D \leq O(\kappa_v^{-1})$, we can within equations (1) and (2) decide how to improve upon the former approximations that $\cos(\alpha - \beta) \approx \cos\alpha$ (assumption 1) and $s_D \approx X_D$ (assumption 2) as follows.

Specifically regarding assumption 1, via Taylor expansion we deduce

$$\frac{\cos\alpha}{\cos(\alpha-\beta)} \approx \frac{\cos\alpha}{\cos\alpha + \beta\sin\alpha} \approx 1 - \beta\tan\alpha \approx 1 - \kappa_v \tan^2\alpha \approx 1 - \kappa_v t_D/(2Y_D) \qquad (9)$$

where $\tan\alpha \equiv \mathrm{d}X_D/\mathrm{d}Y_D \approx \sqrt{t_D/(2Y_D)}$ via equation (7), and where equation (4) has also been used with the approximation $\tan\beta \approx \beta$.

Notice that we are perturbing here assuming that β is much smaller than α (i.e. strong anisotropy) and we think of t_D as being no greater than order κ_v^{-1}. This is distinct from what would happen in the isotropic case [19], for which $\beta = \alpha$ identically, but (for times t_D up to order unity at least) $\cos\alpha$ could itself be expanded assuming the foam front normal is nearly horizontal at early times.

Moreover, returning to the anisotropic case, the location of a material point $\hat{Y}_D$ at some historical time $\hat{t}_D$ (given the point in question is at Y_D at current time t_D) is

$$\hat{Y}_D \approx Y_D + (t_D - \hat{t}_D)\kappa_v/2 \approx Y_D\left(1 + (t_D - \hat{t}_D)\kappa_v/(2Y_D)\right). \tag{10}$$

Regarding assumption 2, the path executed by a material point is

$$s_D = \int_0^{t_D} ((\mathrm{d}X_D/\mathrm{d}t_D)^2 + (\mathrm{d}Y_D/\mathrm{d}t_D)^2)^{1/2}\,\mathrm{d}t_D = \int_0^{X_D}\left(1 + \frac{(\mathrm{d}Y_D/\mathrm{d}t_D)^2}{(\mathrm{d}X_D/\mathrm{d}t_D)^2}\right)^{1/2}\mathrm{d}X_D \tag{11}$$

which after a Taylor expansion plus some algebra via equations (5), and (8), and subsequently equation (6), leads to

$$s_D \approx \int_0^{X_D}\left(1 + \frac{1}{2}\frac{\kappa_v^2/4}{(Y_D^2/X_D^2)}\right)\mathrm{d}X_D \approx X_D(1 + \kappa_v^2 X_D^2/(24Y_D^2)) \approx X_D(1 + \kappa_v^2 t_D/(12Y_D)) \tag{12}$$

and hence $X_D/s_D \approx 1 - \kappa_v^2 t_D/(12Y_D)$. This exhibits only second order variation in κ_v, a significant contrast from equations (9) and (10) which are first order in κ_v. This then gives insights into why the results presented here are subtly different from the results for an isotropic system presented in [19]: the isotropic system has $\kappa_v = 1$ and the perturbation variable becomes the time t_D itself instead of κ_v, and equation (12) is now first order in this perturbation variable t_D.

Returning to the anisotropic system, we note that it is possible to write X_D in the form $(\int_0^{t_D}(\mathrm{d}X_D^2/\mathrm{d}t_D)\,\mathrm{d}t_D)^{1/2}$ where $\mathrm{d}X_D^2/\mathrm{d}t_D = 2X_D\mathrm{d}X_D/\mathrm{d}t_D = 2(X_D/s_D)\,s_D\mathrm{d}X_D/\mathrm{d}t_D$, and where $\mathrm{d}X_D/\mathrm{d}t_D$ is given by equation (1). Substituting equations (9) and (10) and (12) into (1), and assuming $t_D \le O(1/\kappa_v)$, and retaining terms through to first order in κ_v, the solution for X_D becomes (in lieu of the Velde solution)

$$\begin{aligned}
X_D &= \sqrt{2\int_0^{t_D}\hat{Y}_D(1 - \kappa_v\hat{t}_D/(2Y_D))\,\mathrm{d}\hat{t}_D} + O(\kappa_v^2)\\
&\approx \sqrt{2\int_0^{t_D} Y_D(1 + \kappa_v t_D/(2Y_D))(1 - \kappa_v\hat{t}_D/(2Y_D))\,\mathrm{d}\hat{t}_D} + O(\kappa_v^2)\\
&\approx \sqrt{\int_0^{t_D} 2Y_D\left(1 + (t_D - 2\hat{t}_D)\kappa_v/(2Y_D)\right)\mathrm{d}\hat{t}_D} + O(\kappa_v^2)\\
&= \sqrt{2Y_D t_D} + O(\kappa_v^2)
\end{aligned} \tag{13}$$

where the historical time $\hat{t}_D$ is a dummy variable in the above integrations.

Note the remarkable result that the order κ_v term vanishes upon integration. In other words, the fact (via equation (10)) that $\hat{Y}_D$ was historically a little higher than the current value Y_D by an order κ_v amount (and hence historically had a higher driving pressure difference) is offset by the fact (via equation (9)) that as β tends to increase with increasing κ_v, the projected thickness (along the front normal) of the dissipative wet foam zone actually increases (keeping the front thickness along the instantaneous propagation direction constant) – this increases the dissipation seen by the front. Only perturbations at order κ_v^2 survive. This explains why in [16] the numerically computed front shapes for $\kappa_v = 0$, $\kappa_v = 0.01$ and $\kappa_v = 0.1$ are all so close to one another (and distinct from the case $\kappa_v = 1$).

We have already commented that the Velde solution corresponding to $\kappa_v \to 0$ leads to poor reservoir sweep. Clearly increasing κ_v to small but finite values does not improve the reservoir sweep, at least not at first order in κ_v and not for times $t_D \leq O(\kappa_v^{-1})$ (which is the time domain corresponding to the validity of the current approximation). It is interesting however to understand how κ_v might affect the front shape and hence reservoir sweep for longer times, and this we address next.

6. Long-time asymptotic behaviour of front shape

Given our prediction that material points migrate downwards with vertical velocity component $-\kappa_v/2$, all points on the front below height $1 - \kappa_v t_D/2$ must have been continuously on the front since time zero, whereas all points above height $1-\kappa_v t_D/2$ must have been newly introduced since time zero. As these newly introduced points start to dominate a greater and greater proportion of the front, it is interesting to speculate whether the front settles into some quasisteady shape, and if so, how the value of κ_v affects the reservoir sweep in that quasisteady system. As we will see, an analytical formula is available for the quasisteady front shape, and the lower the value of κ_v, the poorer the reservoir sweep becomes.

Noting that the top of the front $Y_D = 1$ is invariably at location $X_D = \sqrt{2t_D}$ [13], we define a coordinate ξ to equal $X_D - \sqrt{2t_D}$. In other words ξ (which for points below $Y_D = 1$ is less than zero according to our sign convention) is the horizontal displacement of a point on the steady front relative to the leading edge at the top. We can make the

assumption (as was done in the analogous solution for isotropic permeability systems at long times [13]), that all points on the front (with the exception of those very near the bottom which are barely moving at all) have displaced through nearly the same distance as the leading edge, i.e. $s_D \approx \sqrt{2t_D}$ uniformly along the front (in lieu of assumption 2): as t_D becomes arbitrarily large, the leading edge at the top of the front has advanced arbitrarily far, and provided points at finite depth remain just a finite distance behind that leading edge, in relative terms the path length they have executed is very nearly the same as that of the leading edge. Despite assumption 2 having been replaced, assumption 1 still applies. In this case (defining $\mathrm{d}\xi/\mathrm{d}Y_D$ to represent a derivative along the foam front from material point to material point at a given time) we deduce

$$\frac{\mathrm{d}\xi}{\mathrm{d}Y_D} = \frac{\mathrm{d}X_D/\mathrm{d}t_D - 1/\sqrt{2t_D}}{\mathrm{d}Y_D/\mathrm{d}t_D} = \frac{(Y_D-1)/\sqrt{2t_D}}{-(Y_D/\sqrt{2t_D})\tan\alpha\ \kappa_v} = \frac{1-Y_D}{Y_D\tan\alpha\ \kappa_v}. \tag{14}$$

Notice however that $\tan\alpha \equiv \mathrm{d}\xi/\mathrm{d}Y_D$ (by definition) and hence

$$\tan\alpha\ \kappa_v \equiv \frac{\mathrm{d}\xi}{\mathrm{d}Y_D}\kappa_v = \sqrt{\frac{1-Y_D}{Y_D}}\sqrt{\kappa_v}. \tag{15}$$

For a typical Y_D between 0 and 1, we deduce $\tan\alpha\ \kappa_v$ (which is also, by definition, $\tan\beta$ according to equation (4)) is an order $\sqrt{\kappa_v}$ quantity, and hence β is small (except within a distance κ_v of the bottom boundary, where the front is barely moving at all, making its local shape of less interest here).

It is easiest to integrate the right hand side of equation (15) via the substitution of a variable ψ such that $Y_D = \cos^2\psi$, in which case upon integration $\sqrt{\kappa_v}\xi$ evaluates to $\sin\psi\cos\psi - \psi$. Converting back to the original set of variables, we deduce the steady state solution for the front shape to be

$$\sqrt{\kappa_v}\xi = \sqrt{Y_D(1-Y_D)} - \arccos\sqrt{Y_D}. \tag{16}$$

It is easy to check upon differentiating equation (16) that equation (15) is recovered. Equation (16) is plotted in Figure 4. The plot is expressed in the form Y_D vs $\sqrt{\kappa_v}\xi$ which should be universal (i.e. independent of κ_v) as long as $\kappa_v \ll 1$.

The area under the Y_D vs ξ curve is a measure of the region in the system which the foam front has not yet reached (or in other words the part of the system underneath the foam front from which foam has not yet had an opportunity to displace oil). Remembering

that $\xi \leq 0$ here, this area can be computed as $-\int_0^1 \xi \, \mathrm{d}Y_D$, which evaluates (using the same substitution in terms of the variable ψ defined above) to $\pi/(8\sqrt{\kappa_v})$, reinforcing the idea that reservoir sweep is poorer (i.e. more area is left unswept) for smaller κ_v.

It is worth noting that the work of [13] found the unswept area in the analogous isotropic case to be $\pi/4$. The formula for the unswept area in the isotropic case is not therefore the same as what is obtained by extrapolating the small κ_v unswept area all the way to $\kappa_v = 1$. This is unsurprising because the front shapes themselves differ. The small κ_v long-time asymptotic solution assumes $\beta \ll \alpha$ (and hence $\cos\alpha/\cos(\alpha-\beta) \approx 1$) whereas the long-time asymptotic solution in the isotropic case has $\beta = \alpha$ (and hence $\cos(\alpha-\beta) \equiv 1$). In one case we must solve $\mathrm{d}\xi/\mathrm{d}Y_D \approx (1-Y_D)/(Y_D \tan\alpha \, \kappa_v)$ and in the other case we must solve $\mathrm{d}\xi/\mathrm{d}Y_D \approx (1-Y_D\cos\alpha)/(Y_D \sin\alpha)$. It was shown in fact in [13] that the isotropic system ($\kappa_v = 1$) predicts a foam front shape at long times

$$-\xi = -\sqrt{1-Y_D^2} + \log(1/Y_D) + \log\left(1+\sqrt{1-Y_D^2}\right). \tag{17}$$

This is also plotted in Figure 4 and clearly differs from the prediction of equation (16).

7. Long-time asymptotics: Behaviour near bottom of the front

Equation (16) can be Taylor expanded both near the bottom of the front ($Y_D \to 0$), and near the top ($Y_D \to 1$). In these limits explicit formulae (for Y_D vs ξ) instead of implicit formulae (ξ vs Y_D) can be derived, and are considered in this section and the section to follow.

Returning to consider equation (16), in the limit of small $Y_D \ll 1$ (still however with $Y_D \gg \kappa_v$ to ensure β is small via equation (15)) this solution reduces to

$$Y_D \approx \frac{1}{4}\left(\sqrt{\kappa_v}\xi + \frac{\pi}{2}\right)^2, \tag{18}$$

which is also plotted in Figure 4. This suggests that Y_D becomes very close to the bottom boundary of the front at a horizontal distance $\pi/(2\sqrt{\kappa_v})$ behind the leading edge. It is therefore only possible for a steady state front to cover the full range of Y_D (from top to bottom of the front) if the leading edge has advanced by at least this distance. This requires then $\sqrt{2t_D} > \pi/(2\sqrt{\kappa_v})$ or equivalently $t_D > \pi^2/(8\kappa_v)$. This then is the estimated time required to set up a steady state front, which gives further support to the notion that the

Velde solution only survives out to times of order κ_v^{-1} (and is replaced by a steady state front shape thereafter).

8. Long-time asymptotics: Behaviour near top of the front

Having considered the leading order behaviour of equation (16) near the bottom of the front, we turn to consider behaviour near the top. Again employing Taylor expansions this turns out to be

$$\xi \approx -\frac{2}{3}\frac{(1-Y_D)^{3/2}}{\sqrt{\kappa_v}} \tag{19}$$

or equivalently

$$Y_D \approx 1 - \left(-\frac{3}{2}\sqrt{\kappa_v}\xi\right)^{2/3} \tag{20}$$

which again is plotted in Figure 4.

This should be compared and contrasted with the local behaviour of the isotropic, long-time asymptotic solution (as given by [13])

$$\xi \approx -\frac{2\sqrt{2}}{3}(1-Y_D)^{3/2} \tag{21}$$

or equivalently

$$Y_D \approx 1 - \left(-\frac{3}{2\sqrt{2}}\xi\right)^{2/3}. \tag{22}$$

Both equations (19) and (21) indicate that the top boundary condition $\alpha = 0$ is now satisfied, since $\mathrm{d}\xi/\mathrm{d}Y_D$ vanishes at the top, with $\tan\alpha \equiv \mathrm{d}\xi/\mathrm{d}Y_D$. However both equations also indicate a mild singularity in the curvature $\mathrm{d}^2\xi/\mathrm{d}Y_D^2$ (curvature diverges like inverse square root of distance from the top boundary). However owing to the $1/\sqrt{\kappa_v}$ factor in equation (19) in the anisotropic permeability case (with $\kappa_v \ll 1$), it is apparent that this describes a front that curves away from the leading edge much more sharply with depth than equation (21) (for the isotropic permeability case) does, albeit the effect is masked in Figure 4 through plotting Y_D against $\sqrt{\kappa_v}\xi$ instead of against ξ. Had we chosen to plot Y_D vs ξ, this would coincide with our intuition that lower κ_v systems have inferior reservoir sweep properties (i.e. more area left unswept by foam) than those with higher κ_v. This is because increasing κ_v improves reservoir sweep by rapidly populating the depth of the foam front with material points which historically until very recently had enjoyed high displacement velocities at or near the top boundary.

Understanding how the κ_v value affects the rate at which front material points adjacent to the top boundary manage to populate the front at depth can be achieved via an analysis analogous to one already presented in [13], which proceeds as follows. Focussing on the small κ_v system, to a good approximation near the top, where α is small, we deduce via equation (19)

$$\alpha \approx \mathrm{d}\xi/\mathrm{d}Y_D \approx \sqrt{(1-Y_D)/\kappa_v} \tag{23}$$

so that (still in the small α limit, with β also small, and with $s_D \approx \sqrt{2t_D}$ and Y_D not too far from unity) equation (2) becomes

$$\frac{\mathrm{d}Y_D}{\mathrm{d}t_D} \approx -\frac{\alpha}{\sqrt{2t_D}}\,\kappa_v \approx -\sqrt{\frac{(1-Y_D)\kappa_v}{2t_D}}. \tag{24}$$

The solution of this is

$$\sqrt{1-Y_D} \approx \sqrt{\frac{\kappa_v}{2}}\left(\sqrt{t_D}-\sqrt{t_{\mathrm{arb}}}\right)+\sqrt{1-Y_{\mathrm{inst}}} \tag{25}$$

where we assume that Y_D takes some instantaneous value Y_{inst} at some arbitrarily chosen time t_{arb}. Rearranging

$$Y_D \approx 1-\left(\sqrt{\frac{\kappa_v}{2}}\left(\sqrt{t_D}-\sqrt{t_{\mathrm{arb}}}\right)+\sqrt{1-Y_{\mathrm{inst}}}\right)^2. \tag{26}$$

We now set $t_D = t_{\mathrm{arb}} + T$ (T being the time elapsed since the arbitrarily chosen time t_{arb}) and Taylor expand in T

$$Y_D \approx 1-\left(\sqrt{\frac{\kappa_v}{2}}\,\frac{T}{2\sqrt{t_{\mathrm{arb}}}}+\sqrt{1-Y_{\mathrm{inst}}}\right)^2. \tag{27}$$

In the event that Y_{inst} is chosen so as to be exceedingly close to the top boundary (i.e. $1-Y_{\mathrm{inst}} \ll \kappa_v T^2/t_{\mathrm{arb}} \ll 1$), we deduce

$$Y_D \approx 1-\kappa_v T^2/(8t_{\mathrm{arb}}). \tag{28}$$

According to equation (28), the material point which is effectively at the top boundary $Y_D = 1$ at $T = 0$ subsequently separates from the top boundary quadratically (rather than linearly) in elapsed time T, which coincides with the view that points instantaneously at the top boundary must be moving horizontally, not vertically. We notice moreover that we need an elapsed time T of order $\sqrt{t_{\mathrm{arb}}/\kappa_v}$ in order for the material point to have migrated a significant distance away from the top boundary. Remember that t_{arb} is at least as large

as $O(1/\kappa_v)$ ($\pi^2/(8\kappa_v)$ being the minimum time needed to set up the steady state front shape solution). It follows that $1/\kappa_v \ll \sqrt{t_{\rm arb}/\kappa_v} \ll t_{\rm arb}$, so the time for a material point to migrate a significant distance away from the top boundary is much smaller than $t_{\rm arb}$ itself (but is simultaneously much larger than the $\sqrt{t_{\rm arb}}$ time scale that would be needed to achieve migration away from the top boundary for a material point in a system with isotropic permeability – see [13]). The relatively slower migration away from the top boundary for points with anisotropic permeability (compared to their isotropic permeability counterparts) manifests itself (through the mechanisms we have already discussed) in poor reservoir sweep.

9. Conclusions

We have considered the behaviour of the pressure-driven growth model for predicting the evolving shape of a foam front during foam improved oil recovery. Specifically we have considered the case of a highly anisotropic system such that vertical permeability is much smaller than horizontal permeability. We have demonstrated that a solution previously derived by de Velde Harsenhorst and co-workers [16, 17] (describing the case when there is no vertical permeability whatsoever) works remarkably well even in the case of small but finite vertical permeability. The reason for this is that when the front shape is expanded in powers of the vertical to horizontal permeability ratio, all terms that are first order in that ratio cancel out and only second order terms survive. We have also shown that material points have a downward vertical motion superposed on a predominant horizontal displacement. This downward vertical motion is slow when the vertical to horizontal permeability ratio is small, meaning that significant vertical displacements only occur after long times. Nonetheless the implication at long times is that the solution for the front shape is dominated by material points that are introduced from the top boundary and subsequently migrate downwards. This leads also to a quasisteady long-time asymptotic solution for the front shape. The long-time solution does exhibit considerable sensitivity to the vertical to horizontal permeability ratio. Reservoir sweep is demonstrably poor when the vertical to horizontal permeability ratio is small, but improves as the permeability ratio rises.

Systems with low vertical to horizontal permeability ratios thereby present challenges for foam improved oil production, because considerable oil might be left in place even after foam

from the upper part of the foam front reaches a production well. One option for overcoming this is to inject at higher pressure in highly anisotropic reservoirs. When the system is expressed in terms of dimensional variables, this not only increases the velocity of the front but also pushes the bottom of the foam front to far greater depths, such that the relative change in the foam front speed for any given increment in depth is correspondingly less, and the displacement over this same increment of depth becomes more uniform.

Acknowledgements

Discussions with W. R. Rossen, S. J. Cox, G. Mishuris, E. Mas-Hernández, N. Shokri, C. Torres-Ulloa and S. Berres are acknowledged.

References

[1] L. W. Lake, Enhanced Oil Recovery, Prentice Hall, Englewood Cliffs, NJ, 2010.

[2] A. R. Kovscek, C. J. Radke, Fundamentals of foam transport in porous media, in: L. L. Schramm (Ed.), Foams: Fundamentals and Applications in the Petroleum Industry, Vol. 242 of Advances in Chemistry, American Chemical Society, Washington, DC, 1994, Ch. 3, pp. 115–163.

[3] L. L. Schramm, F. Wassmuth, Foams: Basic principles, in: L. L. Schramm (Ed.), Foams: Fundamentals and Applications in the Petroleum Industry, Vol. 242 of Advances in Chemistry, American Chemical Society, Washington, DC, 1994, Ch. 1, pp. 3–45.

[4] W. R. Rossen, Foams in enhanced oil recovery, in: R. K. Prud'homme, S. A. Khan (Eds.), Foams: Theory, Measurements and Applications, Surfactant Science Series, Marcel Dekker, New York, 1996, Ch. 2, pp. 99–187.

[5] D. Shan, W. R. Rossen, Optimal injection strategies for foam IOR, SPE J. 9 (2004) 132–150.

[6] W. R. Rossen, Numerical challenges in foam simulation: A review, in: SPE Annual Technical Conference and Exhibition, New Orleans, LA, 30th Sep.–2nd Oct., 2013, SPE-166232-MS.

[7] C. S. Boeije, W. R. Rossen, Fitting foam-simulation-model parameters to data: I. Co-injection of gas and liquid, SPE Reservoir Evaluation & Engg 18 (2015) 264–272.

[8] W. R. Rossen, C. S. Boeije, Fitting foam-simulation-model parameters to data: II. Surfactant-alternating-gas foam applications, SPE Reservoir Evaluation & Engg 18 (2015) 273–283.

[9] K. Ma, J. L. Lopez-Salinas, M. C. Puerto, C. A. Miller, S. L. Biswal, G. J. Hirasaki, Estimation of parameters for the simulation of foam flow through porous media. Part 1: The dry-out effect, Energy & Fuels 27 (2013) 2363–2375.

[10] K. Ma, R. Farajzadeh, J. L. Lopez-Salinas, C. A. Miller, S. L. Biswal, G. J. Hirasaki, Non-uniqueness, numerical artifacts, and parameter sensitivity in simulating steady-state and transient foam flow through porous media, Transp. Porous Media 102 (2014) 325–348.

[11] K. Ma, G. Ren, K. Mateen, D. Morel, P. Cordelier, Modeling techniques for foam flow in porous media, SPE J. 20 (2015) 453–470.

[12] M. Abbaszadeh, A. Kazemi Nia Korrani, J. L. Lopez-Salinas, F. Rodriguez-de La Garza, A. Villavicencio Pino, G. Hirasaki, Experimentally-based empirical foam modeling, in: SPE Improved Oil Recovery Symposium, Tulsa, OK, 12th–16th Apr., 2014, SPE-169888-MS.

[13] P. Grassia, E. Mas-Hernández, N. Shokri, S. J. Cox, G. Mishuris, W. R. Rossen, Analysis of a model for foam improved oil recovery, J. Fluid Mech. 751 (2014) 346–405.

[14] E. Mas-Hernández, P. Grassia, N. Shokri, Modelling foam improved oil recovery within a heterogeneous reservoir, Colloids and Surf. A, Physicochem. and Engg Aspects 510 (2016) 43–52.

[15] P. Grassia, C. Torres-Ulloa, S. Berres, E. Mas-Hernández, N. Shokri, Foam front propagation in anisotropic oil reservoirs, Eur. Phys. J. E 39 (2016) 42.

[16] R. M. de Velde Harsenhorst, A. S. Dharma, A. Andrianov, W. R. Rossen, Extension

of a simple model for vertical sweep in foam SAG displacements, in: EAGE Annual Conference and SPE EUROPEC, London, UK, 10th–13th Jun., 2013, SPE-164891-MS.

[17] R. M. de Velde Harsenhorst, A. S. Dharma, A. Andrianov, W. R. Rossen, Extension and verification of a simple model for vertical sweep in foam SAG displacements, SPE Reservoir Evaluation & Engg 17 (2014) 373–383.

[18] E. Mas-Hernández, P. Grassia, N. Shokri, Foam improved oil recovery: Modelling the effect of an increase in injection pressure, Eur. Phys. J. E 38 (2015) 67.

[19] P. Grassia, L. Lue, C. Torres-Ulloa, S. Berres, Foam front advance during improved oil recovery: Similarity solutions at early times near the top of the front, Submitted to J. Fluid Mech.

[20] E. Mas-Hernández, P. Grassia, N. Shokri, Foam improved oil recovery: Foam front displacement in the presence of slumping, Colloids and Surf. A, Physicochem. and Engg Aspects 473 (2015) 123–132.

Appendix A. Governing equations in dimensional form

In this appendix, the governing equations for pressure-driven growth [5, 13] are given in dimensional form, the governing equations as used in the main text being dimensionless analogues of these.

In the pressure-driven growth model, a foam front is represented by a multitude of material points which separate surfactant liquid downstream from injected gas upstream. We use the symbol X to denote horizontal location (of a material point on the foam front), Y to denote vertical location (again of a material point), s to denote path length travelled (by a material point), t to denote time, k to denote (horizontal) permeability of the system (with $\kappa_v k$ then denoting the vertical permeability in an anisotropic system), λ_r to denote foam relative mobility (i.e. the reciprocal of effective viscosity), S_w to denote the residual water fraction in the foam and ϕ to denote porosity. Meanwhile we use the symbol ΔP to denote the pressure difference between injection pressure P_{inj} and hydrostatic pressure P_{hyd} (more specifically P_{hyd} is the hydrostatic pressure differential between the surfactant liquid

ahead of the front and the gas in the foam behind it; this grows proportionally to depth, the proportionality coefficient being the product of gravity acceleration g and liquid-to-gas density difference $\Delta\rho$). The wet foam zone that forms at the boundary between surfactant and injected gas, is taken (based on so called fractional flow theory [5]) to have a thickness proportional to the path length travelled, i.e. the thickness is $\tau\, s$ with τ being a small dimensionless parameter (typically on the order of 0.01, although the exact value is sensitive to foam physical chemistry, i.e. the extent to which foam manages to resist collapse). More specifically for an anisotropic system [16], $\tau\, s$ is the thickness of the wet foam zone measured along the direction of motion of foam material points (which is taken to be an angle β from the horizontal). A lesser thickness (see e.g. Figure 2) would be measured along the normal to the front (angle α from the horizontal) and this lesser thickness is $\tau\, s \cos(\alpha - \beta)$.

The governing equations now become [5, 13]

$$\frac{\mathrm{d}X}{\mathrm{d}t} = \frac{k\lambda_r}{(1-S_w)\phi}\,\frac{\Delta P}{\tau\, s\, \cos(\alpha-\beta)}\,\cos\alpha \tag{A.1}$$

$$\frac{\mathrm{d}Y}{\mathrm{d}t} = \frac{k\lambda_r}{(1-S_w)\phi}\,\frac{\Delta P}{\tau\, s\, \cos(\alpha-\beta)}\,\sin\alpha\;\kappa_v. \tag{A.2}$$

Given these equations for the evolution of X and Y, the value of path length s evolves according to $\mathrm{d}s/\mathrm{d}t = ((\mathrm{d}X/\mathrm{d}t)^2 + (\mathrm{d}Y/\mathrm{d}t)^2)^{1/2}$.

The front is assumed to be vertical initially at location $X = 0$ (meaning the front normal is initially horizontal, i.e. $\alpha = 0$ initially, and also $\beta = 0$ initially according to equation (4)). Moreover $s = 0$ initially. The condition $\alpha = 0$ is maintained at the top boundary of the front at all subsequent times. The origin of the vertical coordinate system is set at the maximum depth to which the front penetrates $d_{\max} = P_{\mathrm{inj}}/(g\,\Delta\rho)$: this is the depth at which hydrostatic pressure balances injection pressure. As a consequence, at coordinate location Y, the net pressure difference driving the front $\Delta P = P_{\mathrm{inj}} - P_{\mathrm{hyd}}$ turns out to equal $g\,\Delta\rho\, Y$. Dimensionless equations (1)–(2) in the main text are obtained by scaling distances by $d_{\max}$ (so as to obtain dimensionless variables X_D, Y_D and s_D) and scaling times by a quantity t_{scale} defined as

$$t_{\mathrm{scale}} \equiv \frac{(1-S_w)\phi}{k\lambda_r}\,\frac{d_{\max}^2}{P_{\mathrm{inj}}}\,\tau = \frac{(1-S_w)\phi}{k\lambda_r}\,\frac{P_{\mathrm{inj}}}{(g\,\Delta\rho)^2}\,\tau \tag{A.3}$$

(so as to obtain a dimensionless variable t_D).

Values of the length scale $d_{\max}$ and time scale t_{scale} are of course sensitive to how the foam improved oil recovery process is operated, and depend also on reservoir and injected fluid properties. However estimates in the literature for a 'typical' case [20] suggest $d_{\max}$ could be on the order of 265 m (assuming a 2.4×10^6 Pa injection pressure) but possibly as much as 2200 m (see [16], assuming an order of magnitude larger injection pressure and somewhat different liquid and gas densities). Meanwhile [20] estimated that t_{scale} could be on the order of 11 days (assuming the injection pressure 2.4×10^6 Pa as given above). Note also the curious result that t_{scale} actually grows with injection pressure, at least according to (A.3). This is counter-intuitive because higher pressure makes the foam front advance faster over any given distance. Nonetheless higher pressure also increases $d_{\max}$ and it turns out [13] that t_{scale} is defined such that at time $t_{\text{scale}}/2$, the top of the front should have advanced horizontally by an amount $d_{\max}$. Moreover the further the front advances the slower it moves.

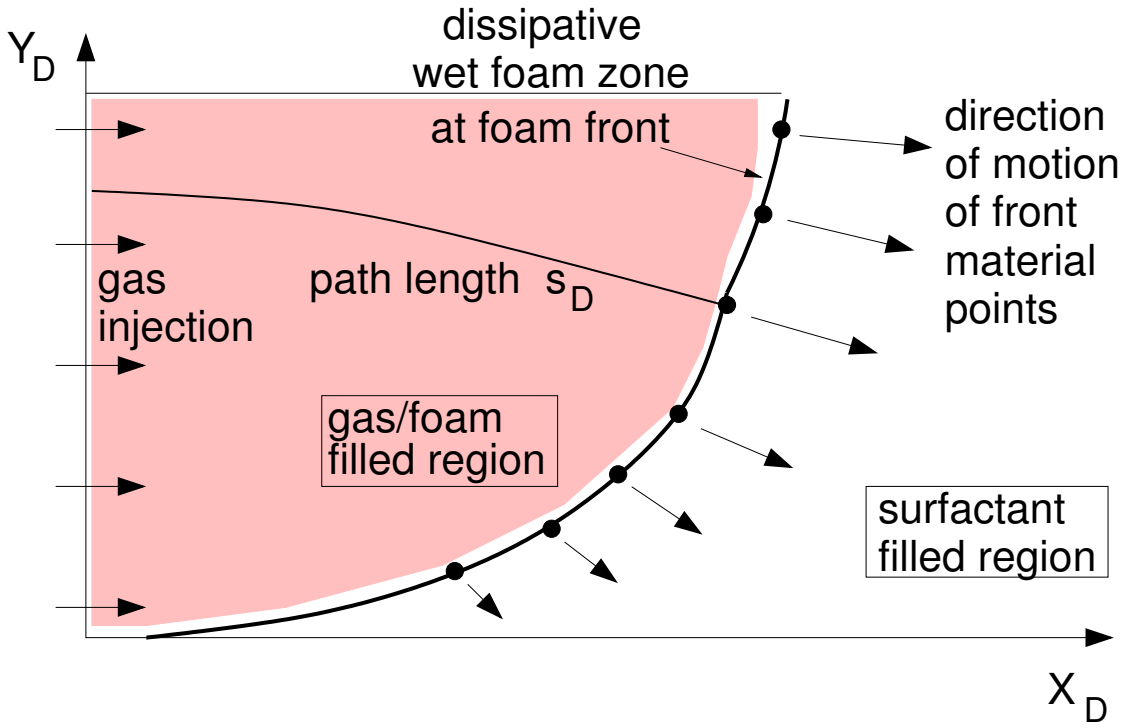

Figure 1: Definition sketch for pressure-driven growth. The dissipative wet foam zone at the foam front separates surfactant liquid downstream from a gas filled region upstream. The front at any instant in time t_D is represented by a set of material points (indicated by black circles) with coordinates (X_D, Y_D), these material points having displaced through a path of length s_D.

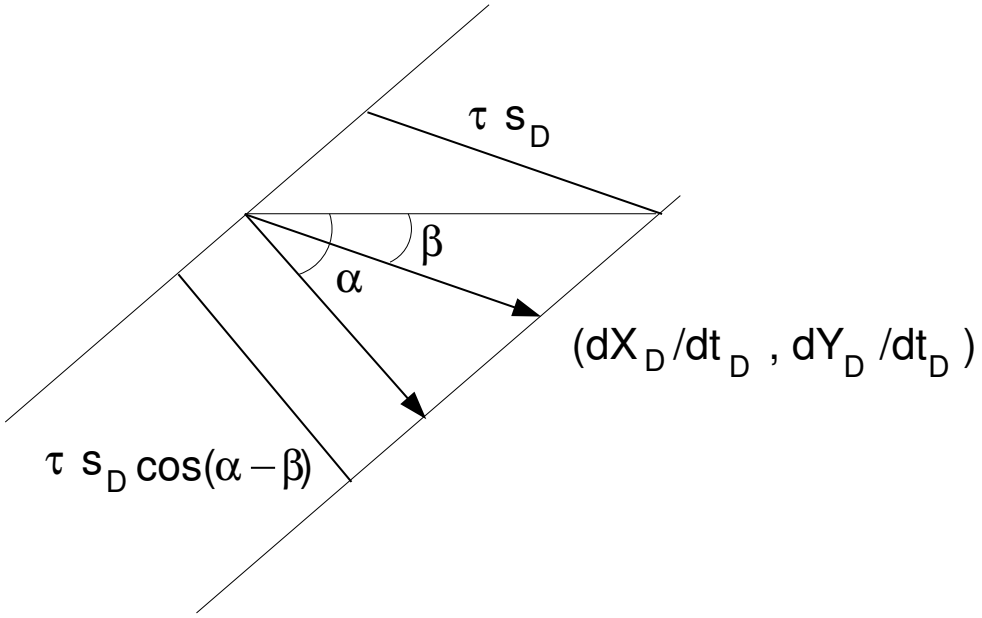

Figure 2: Zoomed view of a local section of foam front, where the normal to the front is at angle α from the horizontal. The velocity vector of a material point $(\mathrm{d}X_D/\mathrm{d}t_D, \mathrm{d}Y_D/\mathrm{d}t_D)$ is at angle β from the horizontal. Here $\beta < \alpha$ in an anisotropic system so the motion of material points is oblique to the front normal. The thickness of the front measured along the velocity direction is $\tau\, s_D$ where τ is a small parameter and s_D is the path length travelled. The thickness of the front measured along the front normal is a factor $\cos(\alpha - \beta)$ smaller.

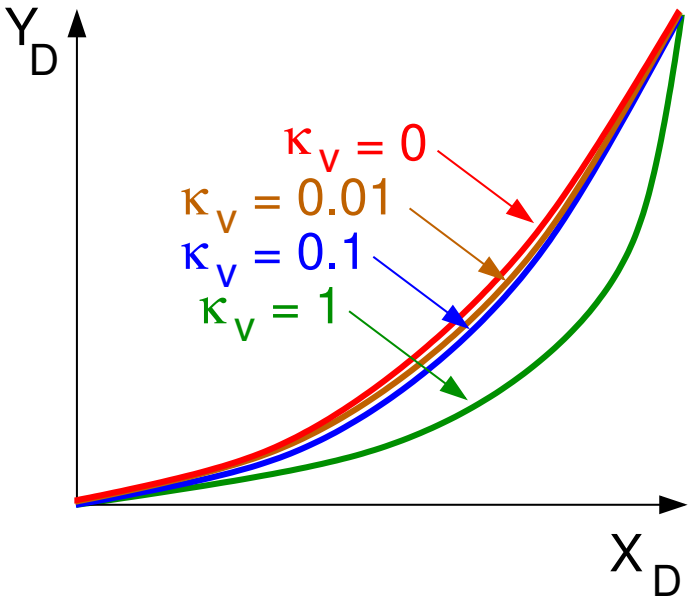

Figure 3: A schematic representation of the typical foam front shapes which were determined numerically by [16]. Data for cases with strong anisotropy ($\kappa_v = 0$, $\kappa_v = 0.01$ and $\kappa_v = 0.1$) were found to be all very close to one another, but differed substantially from the isotropic case ($\kappa_v = 1$). To view the graph showing the original numerical data, refer to [16].

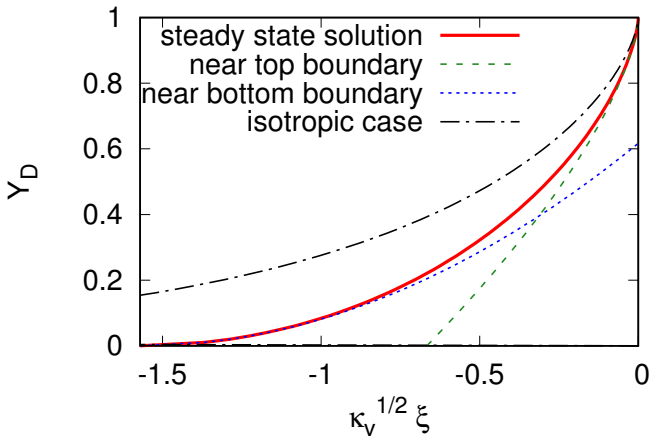

Figure 4: Steady state front shape predicted for a highly anisotropic permeability, showing also the leading order behaviour near the top and bottom boundaries. A comparison with the steady state front shape in the isotropic case is also shown.